Shock Waves (2008) 17:387–395
DOI 10.1007/s00193-008-0129-y

ORIGINAL ARTICLE

Shock pattern in the plume of rocket nozzles: needs for design consideration

Gerald Hagemann · Manuel Frey

Received: 9 October 2007 / Accepted: 27 February 2008 / Published online: 1 April 2008

Abstract For ideal nozzles, basically two different types of shock structures in the plume may appear for overexpanded flow conditions, a regular shock reflection or a Mach reflection at the nozzle centreline. Especially for rocket propulsion, other nozzle types besides the ideal nozzles are often used, including simple conical, thrust-optimized or parabolic contoured nozzles. Depending on the contour type, another shock structure may appear: the so-called cap-shock pattern. The exact knowledge of the plume pattern is of importance for mastering the engine operation featuring uncontrolled flow separation inside the nozzle, appearing during engine start-up and shut-down operation. As consequence of uncontrolled flow separation, lateral loads may be induced. The side-load character strongly depends on the nozzle design, and is a key feature for the nozzle's mechanical structure layout. It is shown especially for the VULCAIN and VULCAIN 2 nozzle, how specific shock patterns evolve during transients, and how - by the nozzle design - undesired flow phenomena can be avoided.

Keywords Rocket engine · Rocket nozzle · Shock wave · Shock shock interaction

Communicated by K. Hannemann.

This paper is based on the invited lecture presented by the first author at the 26th international symposium on shock waves, Göttingen, Germany, July 15–20, 2007.

G. Hagemann (✉) · M. Frey
Astrium Space Transportation GmbH,
Propulsion and Equipments,
81663 Munich, Germany
e-mail: Gerald.Hagemann@astrium.eads.net

M. Frey
e-mail: Manuel.Frey@astrium.eads.net

PACS 47.40.Ki · 47.40.-x

1 Introduction: rocket nozzle contours and plume pattern

Rocket engine thrust chamber design requirements typically include high performance demands at minimum weight in a specified, limited geometric envelope. Thus, a derived nozzle requirement asks for maximum thrust contribution at a given nozzle length. Different types of rocket nozzle contours are applied by space propulsion industry to master the design challenges. The classical design approach is based on ideal contours (designed with method of characteristics, delivering a homogeneous 1-D exit profile), but being significantly truncated to limit overall thrust chamber length. As of today, practically all Eastern world rocket engines are designed with truncated ideal contours; examples are the Japanese LE-7 and the Russian RD-0120. Hoffman [1] proposed in 1985 a design approach for further shortening truncated ideal nozzles without significantly altering performance, by linear compression. This approach was recently adopted for the successor of the LE-7 engine, the LE-7A engine.

In 1959, Rao [2] formulated a direct optimisation approach to maximise performance for a prescribed nozzle length, based on the method of characteristics. Later, Rao simplified this design approach by showing that thrust-optimised contours are very similar to rather simple parabolic contours [3]. This approach has been adopted in the majority of western world rocket engines, including the American SSME and RS-68, and the European VULCAIN and VULCAIN 2.[1]

[1] The VULCAIN and VULCAIN 2 engines have been developed by Snecma Safran in France, which shared the development with partners in Europe.

Table 1 Characteristic rocket engine data

Engine	Launcher	Chamber pressure (bar)	Nozzle area ratio	Thrust (vacuum) (KN)	Specific impulse (vacuum) (s)
VULCAIN	ARIANE 5 G	110	45	1,145	431
VULCAIN 2	ARIANE 5 ECA	115.5	59, with TEG-injector at 32	1,350	434
LE-7	H-II	127	54	1,078	446
LE-7A	H-II A	121	52 (original), 39 (modified), with H_2-injection at 36	1,098	436
RD-0120	Energia	218	85.7	1,961	455
SSME (Bl. II)	Space shuttle	204	77.5	2,278	453
RS-68	Delta IV	97	21.5	3,313	410

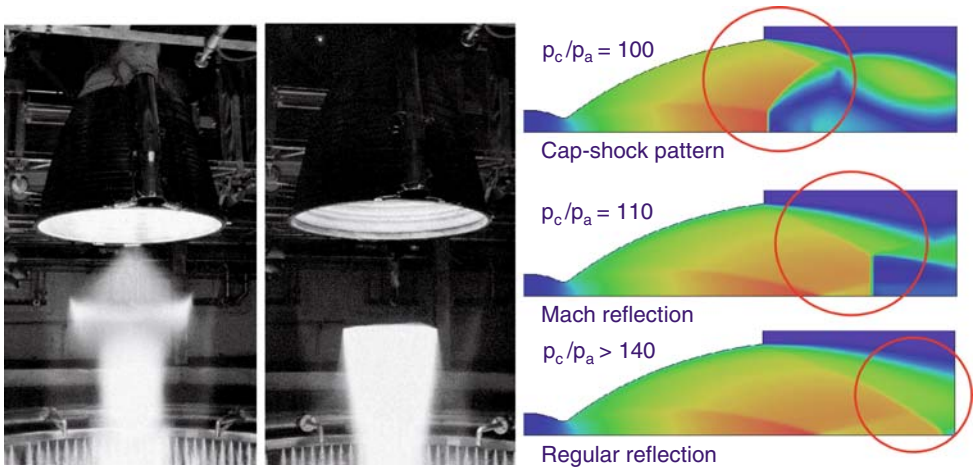

Fig. 1 Nozzle plume pattern observed in the VULCAIN engine: cap-shock pattern (*left*) and classical Mach disk (*center*). Numerical simulations (*right*), also with regular reflection (*bottom right*) (Mach number distribution, increasing from *blue to red*)

Table 1 summarises characteristic data of the above mentioned engines. These booster- and main stage engines feature rather high area ratio nozzles to maximise engine performance during high altitude and hence vacuum flight phases. Except for the RS-68, the nozzle area ratios have been maximised, but facing the constraint of sufficient margin against uncontrolled flow separation. For nominal load point operation at sea-level, this leads to an effectively full-flowing nozzle extension. The supersonic exhaust gases are highly overexpanded, and are re-compressed behind the nozzle exit by means of shocks to the ambient pressure condition.

It is obvious that the divergent nozzle contour directly influences the nozzle plume pattern. The plumes of ideal plane and axisymmetric supersonic expansion nozzles are frequently discussed in the literature, e.g. [4–6]. Depending on the contour type and the operational condition as influencing factors, three different plume patterns may be observed in the highly overexpanded plume: the regular shock reflection,[2] the Mach reflection, and/or the so-called cap-shock pattern.

Figure 1 shows two photographs of the VULCAIN engine during ground operation. At nominal chamber pressure operation, the nozzle extension generates a highly overexpanded flowfield, with an average 1-D exit pressure of approximately. 0.18 bar. The exhaust gases are recompressed to ambient pressure. The cap-shock pattern (left photo) and the classical Mach disk (right photo) are observed in the plume of VULCAIN [8,9].

Figure 1 also illustrates the VULCAIN engine plume pattern simulated by CFD analysis for different pressure ratios from chamber pressure to ambient pressure, featuring all three plume patterns. For the lower pressure ratio, the cap-shock pattern appears in the plume. For increasing pressure ratios, transition to the Mach reflection with its characteristic disk is observed. The numerical simulations compare well for the two photographs from engine test with cap-shock pattern and Mach disk. For even higher pressure ratios (which cannot be reached on ground operation due to fixed ambient pressure and limitations on max. chamber pressure), the regular reflection will appear and can therefore only be observed during flight.

The regular reflection and the Mach reflection may be observed in the plume of all nozzle types, while the cap-shock pattern can only be observed for nozzles featuring an inter-

[2] Note: for axisymmetric flows, in principle the pure regular reflection does not exist. A small Mach stem appears at the centerline, see e.g. [7]. Here, this apparent regular reflection is referred to as the regular reflection.

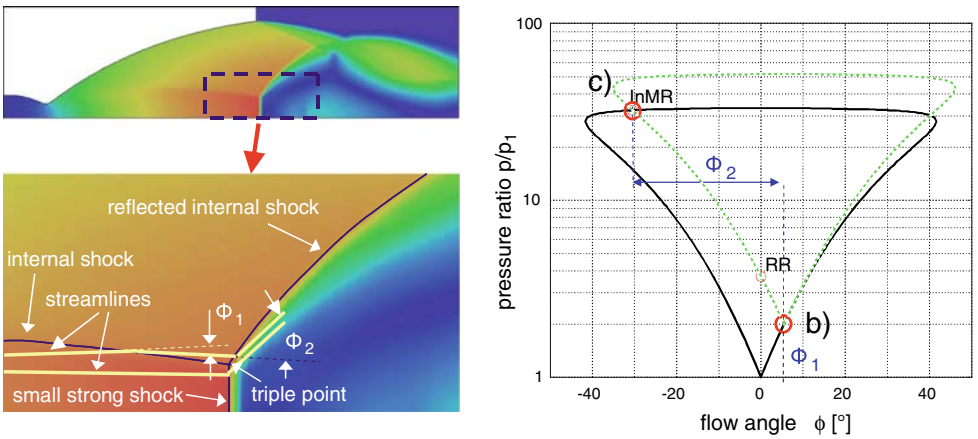

Fig. 2 Analysis of cap-shock pattern by means of pressure deflection diagram by tracking two streamlines, the first (*lower*) with a normal shock path, the second (*upper*) with a double shock path with associated changes in flow path angles Φ_1 and Φ_2

nal shock, such as thrust-optimized, parabolic or compressed truncated ideal nozzles. The internal shock results from the—from a pure aerodynamic point of view—not perfect contour design, and is induced shortly downstream of the nozzle throat at the inflection point in wall curvature with a sudden change from a convex to concave contour shape. At this point, a discontinuity in the wall curvature (second derivative) is present, and the contour downstream with its strong curvature towards the axis induces compression waves finally focussing to the internal shock. With the Mach number distribution shown in Fig. 1, this internal shock can be easily traced inside the nozzle.

Based on analyses performed in the late 90's by the authors, it has been shown that the cap–shock pattern results from the shock–shock interaction between the inverse Mach reflection of the internal shock with the recompression shock. Figure 2 (left) illustrates details of a numerical simulation of the cap-shock pattern and analyzes the flow with the pressure–deflection diagram[3] (Fig. 2 right), due to the shape of its curves often referred to as heart-curve. This diagram shows all possible states the flow can reach by passing a single shock (black heart-curve) or for a given first shock all possible states that can be reached by passing a second shock (dashed green heart-curve). For the cap shock pattern, two streamlines very close to each other are analyzed, one passing slightly above the triple point of the cap shock pattern, the other passing slightly below it, see Fig. 2 left. The streamline slightly below the triple point only passes the small strong shock, hence its downstream state is described by a point on the black heart curve. The streamline slightly above the triple point must pass through two shocks, first the internal shock and then the reflected internal shock. The strength of the internal shock is known, hence the state of the flow of it is known and can be marked on the black heart curve as point (b). The green heart-curve describes the state downstream of any second shock starting at point (b), hence one point on the green heart-curve also describes the state downstream of the reflected internal shock. Two compatibility conditions are applied to derive this flow state: First, both flow direction and pressure must be identical for the two observed streamlines downstream of the shock pattern, i. e. their state is described by one common point in the pressure-deflection diagram. Second, the reflected internal shock is of opposite family compared to the internal shock, therefore the solution must be the left intersection of the two heart-curves in Fig. 2 left, labelled as point (c). Thus, point (c) describes the flow directly downstream of the triple point for both considered streamlines.

This is well in line with the numerical and experimental findings. Associated changes in flow angles for the upper streamline featuring the two shock transitions compare well between CFD solution and the analytical assessment in the pressure–deflection diagram. This analysis indicates that the reflection phenomenon of the internal shock is an inverse Mach reflection (point InMR in Fig. 2); see [5,10] for a detailed discussion on the subject.

The cap-shock pattern and its transition to the Mach reflection are influenced by the contour shape, and by the operational conditions of the thrust chamber. Further, a significant hysteresis is observed for the pressure ratio (chamber to ambient pressure) at the instant of transition between engine start-up (or up-ramping) and shut-down (or down-ramping), see Fig. 3. During start-up at low pressure ratios, the cap-shock pattern is present in picture 1 of Fig. 3). For increasing pressure ratios, the centerline location of the small strong shock of the inverse Mach reflection moves downstream until the point is reached where the internal shock is regularly reflected at the axis. Here, the inverse Mach reflection of the internal shock is transformed into a regular reflection (see picture 2 in Fig. 3). This closes the high

[3] It is noted that the pressure-deflection diagram is only valid for planar flows. The comparison is used here for visualisation only. The resulting uncertainty has been assessed by the authors.

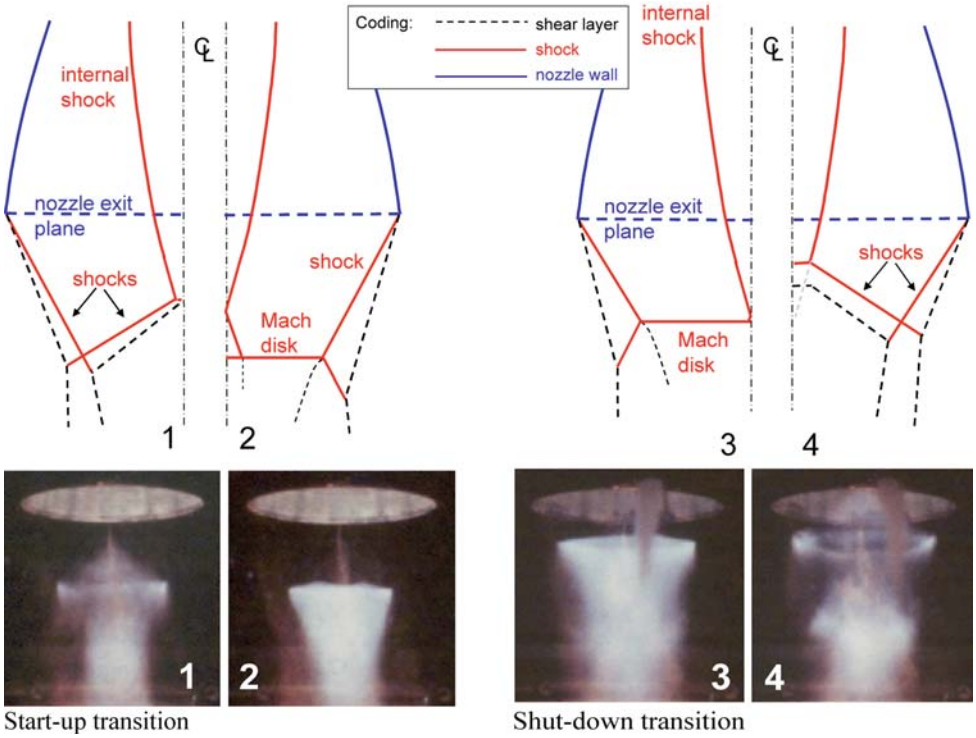

Fig. 3 Transition from cap-shock pattern (1) to Mach disk (2) during start-up (*left*), and from Mach disk (3) to cap-shock pattern (4) during shut-down (*right*). Sketches show only one half of nozzle, being flipped from 1 to 2 and 3 to 4 for direct comparability. Photos taken from high speed video

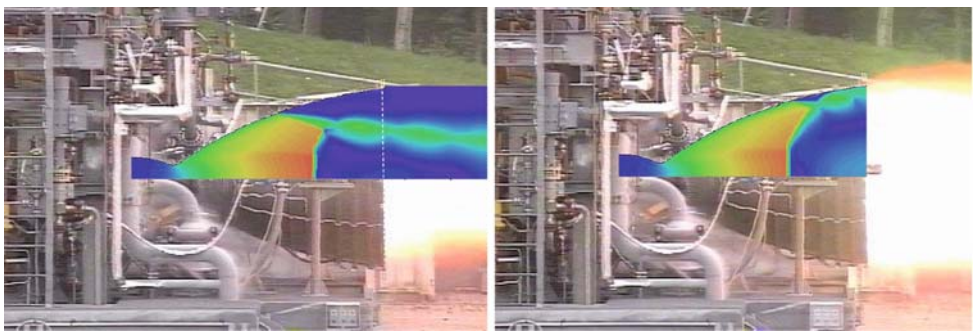

Fig. 4 VULCAIN thrust chamber during start-up (at pressure ratio p_c/p_a of approximately 40), with free shock separation (FSS, *left*) and restricted shock separation (RSS, *right*) (Mach number distribution as inlay, increasing from *blue to red*)

Mach number kernel along the centerline, with lower Mach numbers downstream of the regular reflection point. The shock-shock interaction suddenly disappears, leading to the appearance of the Mach reflection of the overexpansion shock further downstream in the plume. Note that the location of the internal shock depends on the specific heat ratio of the expansion gases, which varies during start-up due to a varying mixture ratio of fuel to oxidizer.

Before shutdown, usually a Mach disk exists, with the internal shock being regularly reflected at the axis (picture 3 in Fig. 3). At shutdown, the Mach disk moves upstream until it reaches the regular reflection point of the internal shock at the axis. From this instant on, the internal shock is again reflected as inverse Mach reflection, hence the overall flow structure changes from Mach disk to cap-shock pattern again. The experimentally observed hysteresis confirms this analysis.

2 Separation and side-load characteristics of rocket nozzles

The exact knowledge of the plume pattern is of special importance for mastering the engine operation with uncontrolled flow separation inside the nozzle, occurring normally only during transient flow conditions, i.e. engine start-up and shutdown operation. As consequence of uncontrolled flow separation, lateral loads may be induced. The side-load character strongly depends on the nozzle design, and is a key load case for the determination of the nozzle's mechanical structure. Principally, two separation patterns are observed, the free shock separation (abbreviated as FSS in the following) and the restricted shock separation (abbreviated as RSS in the following). Both patterns are illustrated in Fig. 4. With FSS, the flow downstream of the separation remains separated from the wall and continues as a free jet. Figure 5 depicts the char-

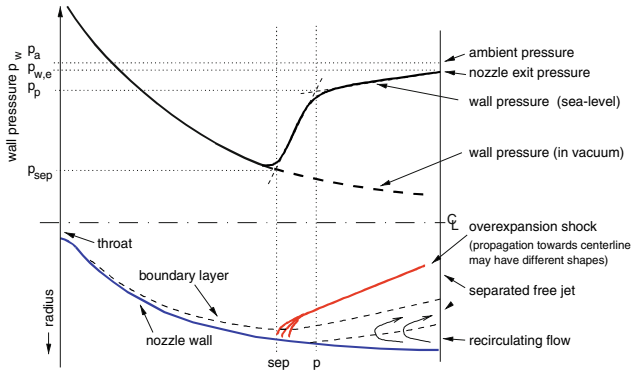

Fig. 5 Characteristics for free shock separation pattern, FSS

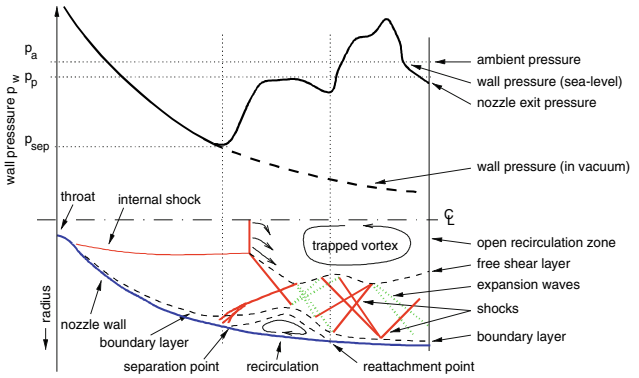

Fig. 6 Characteristics for restricted shock separation pattern, RSS

acteristics of free shock separation. This pattern is observed in any type of overexpanded nozzle, and has been subject to intensive analytical and numerical analyses, [10]. With RSS, the separated flow re-attaches again to the nozzle wall, thus forming a closed separation bubble. Figure 6 depicts the characteristics of restricted shock separation. This separation pattern is driven by the cap-shock pattern, and thus can occur only inside nozzles with an internal shock, such as compressed truncated ideal contours, thrust-optimised and parabolic contours. Key driver for the re-attachment is the momentum balance across the cap-shock pattern, with the radial momentum towards the wall generated by the reflected internal shock as illustrated in Fig. 7. The relative distance of the separation location and the small strong shock at the centreline may be used to characterize the instant of transition.

The criticality of RSS is twofold: first, the transition from free- to restricted shock separation imposes significant impulsive side-loads to be mastered by the lightweight nozzle structure. The re-transition process from RSS to FSS (triggered by the opening of the closed separation bubble as it approaches the nozzle exit) occurs shortly before the full-flowing, and is of oscillative character, associated again with side-loads. And second, the re-attached supersonic flow remaining attached to the wall introduces a significant heat load towards the wall with the risk of local overheating due to significantly

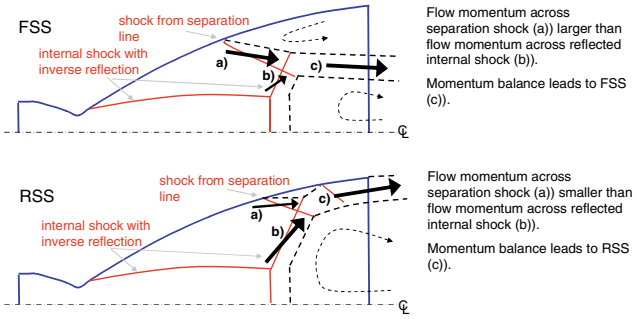

Fig. 7 Momentum balance across cap-shock pattern, as key driver for re-attachment

higher wall pressure caused by shock waves (see also Figs. 6, downstream of reattachment point). Figures 8 and 9 illustrate both critical elements: Fig. 8 includes two photos taken from a hot-firing test with a 40 kN ceramic nozzle demonstrator operated with LOX/H_2. Both photos are taken at approximately the same operational condition with a pressure ratio of approximately $p_c/p_a = 40$. In the left, FSS is shown, with the attached flow condition visualised by the radiation-cooled nozzle wall. In the right, the RSS condition shortly after transition is shown. The excessive heat load for the re-attached condition with RSS is clearly visible inside the radiation-cooled 40 kN ceramic nozzle demonstrator. The re-attached flow region is visualized by the much stronger radiation due to significantly higher wall temperatures, caused by the higher wall pressure.

Figure 9 includes side-load profiles for a truncated ideal nozzle and for a parabolic nozzle, both being recorded from cold gas tests with laboratory scale nozzles [10]. The distinct difference in side-load history is obvious for both nozzle types, with the higher side-load for the thrust-optimized parabolic TOC-nozzle featuring the transition from FSS to RSS and vice versa. The first distinct side-load peak for the TOC-nozzle at approx. $p_c/p_a = 40$ is caused by the first transition from FSS to RSS during start-up. The second distinct side-load peak at approx. $p_c/p_a = 65$ is linked to the re-transition from RSS to FSS, occurring shortly prior to the full-flowing of the nozzle at start-up.

2.1 Characteristics for truncated ideal nozzles: RD-0120, LE-7

In truncated ideal nozzles, only free shock separation occurs. This has also been demonstrated within the European Calo-Programme by means of an extensive test programme with a 40 kN thrust chamber operated with LOX/H_2, see [11]. Key-side load driver are random pressure pulsation in the separation zone. For rocket engines equipped with truncated ideal nozzles such as RD-0120 and LE-7, no major problems with side-loads have been reported. It can be stated in prin-

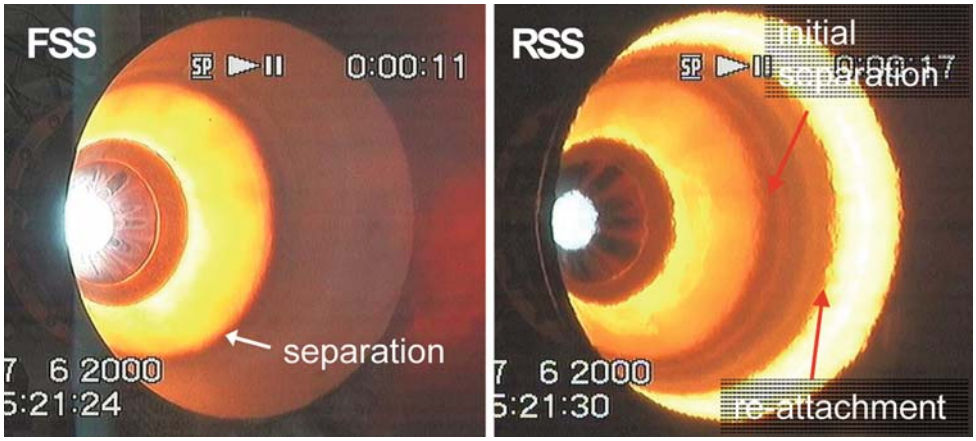

Fig. 8 40 kN thrust chamber flow in FSS- (*left*) and RSS condition (*right*) at pressure ratio of approx. $p_c/p_a = 40$

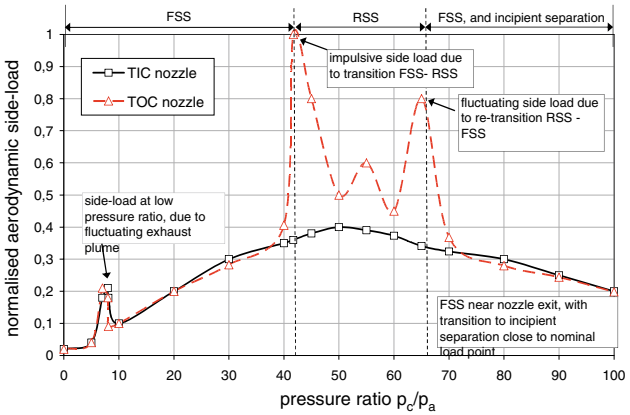

Fig. 9 Typical side-load profile for truncated ideal (*TIC*) and thrust-optimized (*TOC*) nozzle

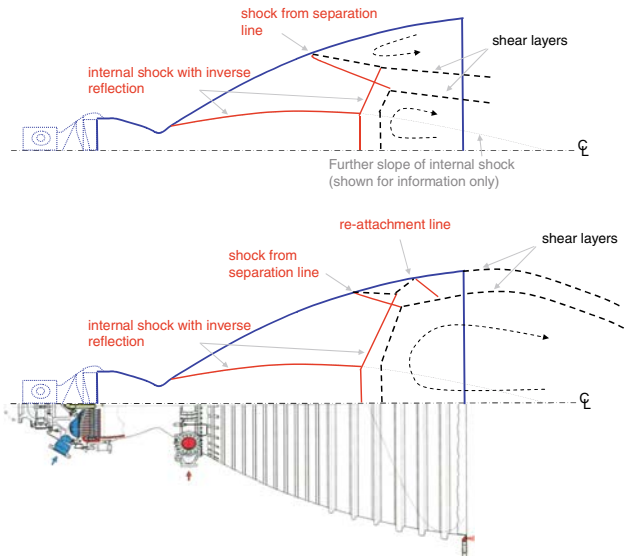

Fig. 10 Nozzle plume pattern observed in the VULCAIN rocket engine: shock pattern evolution during start-up (see also [4]): Free-shock separation up to pressure ratio of approximately $p_c/p_a = 40$ (*top*), and after transition to restricted shock separation at practically same pressure ratio

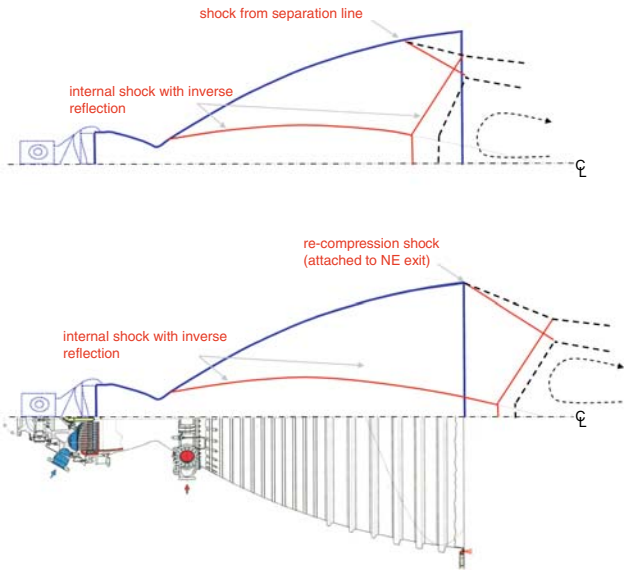

Fig. 11 Nozzle plume pattern observed in the VULCAIN rocket engine: shock pattern evolution during start-up (see also [4]): Re-transition to free shock separation near pressure ratio $p_c/p_a = 65$, and full-flowing achieved for pressure ratios beyond $p_c/p_a = 80$

ciple, that for this nozzle design side-loads are not regarded as critical issue, [10,12].

2.2 Characteristics for thrust-optimized/parabolic nozzles: VULCAIN, SSME

As discussed before, this nozzle type introduces the risk of a change in separation pattern from free- to restricted shock separation. The plume instability shortly before and at its sudden FSS to RSS change is the key side-load driver. Due to its impulsive character, this load case has to be carefully handled within the design. Figures 10 and 11 sketch the shock pattern evolution inside the VULCAIN nozzle extension during start-up. Maximum side-loads induced by the transition process close to a pressure ratio $p_c/p_a = 40$ are assessed to approximately 3% of the vacuum thrust level [9]. The transi-

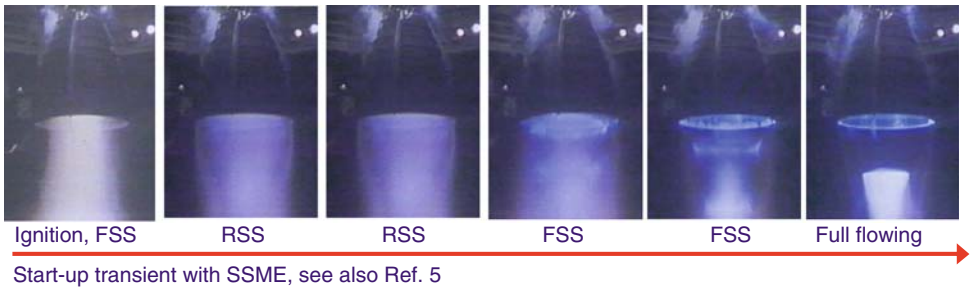

Fig. 12 Nozzle plume pattern observed in the SSME rocket engine: shock pattern evolution during start-up, with free-shock and restricted shock separation

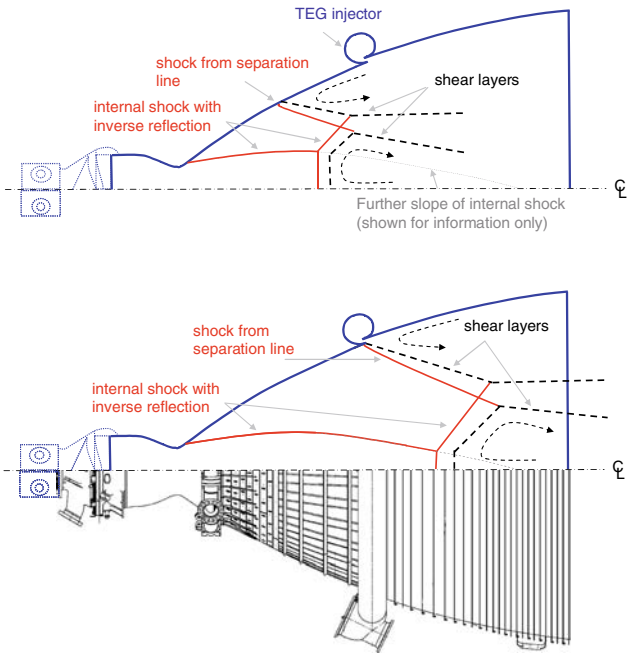

Fig. 13 Nozzle plume pattern in the VULCAIN 2 rocket engine: shock pattern evolution during start-up: FSS, with cap-shock far inside nozzle (*top*); and FSS, with cap-shock inside nozzle, and separation stabilized at TEG-injector (*bottom*)

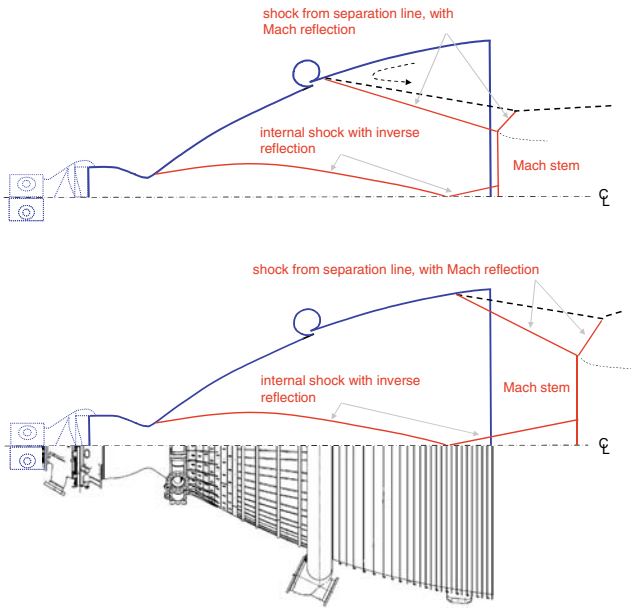

Fig. 14 Nozzle plume pattern in the VULCAIN 2 rocket engine: shock pattern evolution during start-up: FSS, with transition to Mach reflection of separation shock, while separation stabilized at TEG-injector (*top*); and Mach reflection of separation shock shortly prior to full-flowing (*bottom*)

tion process, and the re-transition process from restricted to free shock separation are also the key side-load drivers inside the SSME engine, based on the analysis of the authors. This finding is in line with a reported SSME nozzle failure due to side-loads, likely to be caused by the oscillative re-transition from restricted shock separation to free shock separation, [13]. The picture sequence shown in Fig. 12 summarises the transition and re-transition inside the SSME nozzle during start-up.

2.3 Thrust-optimized/parabolic nozzle without RSS: VULCAIN 2

The transition from FSS to RSS is driven by the momentum balance across the cap-shock pattern. Consequently, the nozzle designer has the chance to avoid the transition process by design in such way, that the momentum balance yields always a balance in favour of FSS. This may be achieved by stabilizing the separation point movement during the critical pressure ratios. For example, in VULCAIN 2 the transition from FSS to RSS does not occur due to separation stabilization at the turbine exhaust gas (TEG) injector. With the TEG-injector, turbine exhaust gases are introduced into the nozzle for performance and cooling reasons, being a design element available with open cycle engines. It is noted that RSS would occur for a clean nozzle wall without TEG-injector. The following sequencing of the flowfield occurs for increasing chamber pressure, see also Figs. 13 and 14

- During start-up, FSS occurs for lowest chamber pressures until separation reaches TEG-injector.
- While FSS separation line is stabilized at the TEG-injector, cap-shock structure moves further downstream towards the nozzle exit, with further increasing chamber pressure.
- Due to specific shape of internal shock (being reflected at centreline inside the nozzle), cap-shock disappears while separation starts to leave the TEG-injector. Maximum

Fig. 15 Nozzle plume pattern observed in the VULCAIN 2 rocket engine: classical Mach disk (with nominal skirt, *right*, and cut skirt, *center*) and cap-shock pattern (with cut skirt, *left*) [Courtesy Snecma Safran, DLR]

side-loads are generated by an asymmetric detachment of the flow from the TEG-injector.
- Further separation appears in FSS condition until incipient separation is reached at nozzle exit, with classical Mach disk in plume.

Figure 15 includes three images taken during the early development of the VULCAIN 2 engine. As shown in the picture to the right, the classical Mach disk is visible at nominal operation under sea-level condition with the full length nozzle extension. Early within the development programme, specific tests with shortened skirt were performed to validate the engine performance at rather low combustion chamber pressure. During the transient start-up, high speed photographs were taken to visualise the plume pattern. The left and center picture are extracted, and prove the existence of the cap-shock pattern for low-level off-design points.

2.4 Characteristics for compressed truncated ideal nozzles with RSS: LE-7A

Due to the internal shock induced in compressed truncated ideal nozzles, this design introduces also the risk of a change in separation pattern from free to restricted shock separation. Thanks to the documentation of the challenges encountered with the LE-7A, it is shown how significant the RSS appearance can be, if not adequately considered within the design [12]. Major problems occurred during engine development due to the appearance of RSS causing local overheating of the nozzle wall. Further problems were encountered by large side-loads, due to an asymmetric movement of the separation line from the rear-mounted H_2-film-injector. The film-injector is closely mounted to the nozzle exit to enable a dismounting of the skirt for low chamber pressure operation. Profound analyses, also by means of subscale tests, were performed to understand and successfully master the design problem. As first countermeasure, the nozzle was significantly cut from area ratio 59 down to 39 to avoid the origin of the large side-loads, the asymmetric detachment.

3 Conclusion

Rocket nozzles belong to the critical components of a rocket engine, being exposed to extreme aerodynamic, thermal and mechanical loads during both transients and steady-state. When changing the design from classical truncated ideal design to other contour types allowing further length reduction, the correct knowledge on separation pattern and associated side-loads is of significant importance. Especially for restricted shock separation, the excessive heat load associated with the re-attached supersonic flow at the nozzle wall and the side-load character has to be mastered by the thermo-mechanical design. It has also been shown that by design, the risk of separation pattern transition may be diminished.

References

1. Hoffman, J.D.: Design of compressed truncated perfect nozzles. AIAA-85–1172 (1985)
2. Rao, G.V.R.: Exhaust Nozzle Contours for Optimum Thrust. Jet Propuls. **28**(6), 377–383 (1958)
3. Rao, G.V.R.: Approximation of optimum thrust nozzle contours. ARS J. **30**(6), 561 (1960)
4. Moelder, S., Gulamhussein. A., Timofeev, E., Voinovich, P.: Focusing of conical shocks at the centreline of symmetry. In: Proceedings of the 21st International Symposium on Shock Waves (1997)
5. Frey, M.: Behandlung von Strömungsproblemen in Raketendüsen bei Überexpansion. Ph.D. Dissertation, Institute of Aerodynamics and Gasdynamics, University of Stuttgart (2001)
6. Shapiro, A.H.: Compressile Fluid Flow. Wiley, New York (1953)
7. Moelder, S., Gulamhussein, A., Timofeev, E., Voinovich, P.: Focusing of conical shocks at the centreline of symmetry. In: Proceedings of the 21st International Symposium on Shock Waves (1997)
8. Hagemann, G., Immich, H., Nguyen, T., Dumnov, G.: Rocket engine nozzle concepts. Liquid rocket thrust chambers: aspects of modeling, analysis, and design. Progr. Astronaut. Aeronaut. vol. **200**, 437–467 (2004)

9. Terhardt, M., Hagemann, G., Frey, M.: Flow Separation and side-load behaviour of the VULCAIN engine. AIAA 99–2762 (1999)
10. Hagemann, G., Frey, M., Koschel, W.: On the appearance of restricted shock separation in rocket nozzles. J. Power Propuls. **18**(3), 577–584 (2002)
11. Hagemann, G., Preuss, A., Grauer, F., Frey, M., Kretschmer, J., Ryden, R., Jensen, K., Stark, R., Zerjeski, D.: Flow separation and heat transfer in high area ratio rocket nozzles. AIAA-2004-3684 (2004)
12. Watanabe, Y., Sakazume, N., Yonezawa, K., Tsujimoto, Y.: LE-7A engine nozzle separation phenomenon and the possibility of RSS suppression by the step inside the nozzle. AIAA-2004–4014 (2004)
13. Goetz, O., Monk, J.: Combustion device failures during space shuttle main engine development. In: Proceedings of the 5th International Symposium on Long Life Combustion Device Technologies, Chattanooga. 27–30 October 2003